Eur. Phys. J. Spec. Top. (2026) 235:9265–9290
https://doi.org/10.1140/epjs/s11734-026-02340-9

THE EUROPEAN PHYSICAL JOURNAL SPECIAL TOPICS

Regular Article

Quantum-inspired density-matrix recurrence analysis of brain time series

Maria Mannone[1,2,3,4,a] and Norbert Marwan[2,3,5]

[1] ICAR, National Research Council of Italy (CNR), Palermo, Italy
[2] Institute of Physics and Astronomy, University of Potsdam, Potsdam, Germany
[3] Potsdam Institute for Climate Impact Research (PIK), Member of the Leibniz Association, Potsdam, Germany
[4] DSMN, Ca' Foscari University of Venice, Venice, Italy
[5] Institute of Geosciences, University of Potsdam, Potsdam, Germany

Received 31 January 2026 / Accepted 20 April 2026 / Published online 9 May 2026
© The Author(s) 2026

Abstract Recurrence analysis allows the investigation of self-similarities in time series. Different degrees of regularity of behaviours, or different typologies of chaos, help characterise physical phenomena whose properties are expressed by time series. We consider here the special case of time series of human brain activity in the insula, an area particularly relevant for emotional and cognitive processing. Starting from time series obtained using functional magnetic resonance imaging, we adopt recurrence plots to investigate differences between normal and selected pathological behaviours. We also present a technique to encode time series into quantum-inspired states, by constructing a density matrix via a kernel mapping. Recurrence structures are derived from similarities between the components of its principal eigenvector. The obtained results highlight differences in behaviour between the time series. Overall, this conceptual study bridges ideas from nonlinear physics, quantum physics, and medical physics.

1 Introduction

Being in a state, departing from it, and then coming back: this is the core idea behind the study of recurrence. A time series constitutes the starting point. Each time that a value returns, or is particularly close (distance within a given threshold), it is marked as a *recurrence*. Once the recurrence matrix is found, different measures can be performed. Visualisation via recurrence plots helps identify patterns of behaviour between periodic, aperiodic, and various chaotic behaviours in nature [14].

Today, recurrence analysis [33, 35, 43], and in particular its graphic tools such as recurrence plots and recurrence networks, are widely applied to a variety of real-life data, including medical data, for instance cardiovascular variability [36, 45, 54], or epilepsy [19, 39].

Here, we focus on a particular typology of time series, the one describing brain activity in terms of brain area activation. The more a brain area is active, the more sugar and oxygen it needs, brought by the blood. Thanks to the paramagnetism of deoxygenated haemoglobin (the oxygenated hemoglobin is diamagnetic), blood movements are detected. This is the basis of the BOLD (blood-oxygenation-level–dependent imaging) signal [8], measured with functional magnetic resonance (fMRI), assessing the activity of brain areas, in particular at resting state. The areas are found through a parcellation of the voxel of brain imaging, depending upon the choice of a medical atlas (here: Automated Anatomic Atlas, AAL [51]).

In this article, we focus on a specific area of the human brain, the (left) *insula*, comparing time series of different selected brains through recurrence analysis. The insula has a relevant role for emotion processing [55] that is structurally and functionally altered in some diseases, such as schizophrenia [49]. Its alteration [2] can affect action

[a] e-mails: maria.mannone@icar.cnr.it; maria.mannone@uni-potsdam.de (corresponding author)

and emotion in Parkinson's disease [3] and other neurodegenerative diseases, such as Alzheimer–Perusini's disease[1] (AD) [5].

Finally, we propose a quantum encoding of the time series. We introduce quantum-inspired recurrence built from the density matrices of encoded time series. This is a mathematical technique, because we make no claim in any way that there is a quantum activity within the brain. Instead, we develop a quantum heuristics. From the quantum states, we compute the *density matrix* via a kernel mapping. Then we compute its principal eigenvector, and from the similarities between its components, we define a new recurrence matrix. We can thus compare plots and measures of the quantum-encoded time series with those of the original ones.

This article is organised as follows. In Sect. 2, we present some literature in the considered domains. In Sect. 3, we present the classical and the quantum method of recurrences, and their application to insula time series is presented in Sect. 4. After the discussions (Sect. 5), we present our conclusions (Sect. 6). Appendix I shows further visualisations of intermediate steps, and Appendix 2 summarises an encoding (without recurrence) of the whole connectivity matrix of the brain within a quantum graph state, a concept recently proposed for weighted networks [18], that, to the knowledge of the authors, has never been applied to medical real data.

2 Related works

The concept of *quantum recurrence* was first proposed in 1957 [4], and more modern works explore Poincaré recurrence and quantum revival [22]. More recently, some studies explored state-independent recurrences in Floquet systems [1].

While several quantum-based studies avoid any reference to recurrence [13], other works, in the realm of classical, nonlinear physics, make use of the concept of *density* without, however, considering the quantum one. It is the case of [25], with density-based recurrence measures from microstates, which are small submatrices of the recurrence matrix. The histograms defined on them allow us to obtain probabilistic measures of determinism and laminarity.

As another precedent of our research, we mention the work in [20], where the temporal evolution of a system is described via a sequence of probability density functions $\{\rho_t^x\}_{t=1}^N$, where each $\rho_t^x(x)$ "encodes the believes about the likelihood of value $X = x$ at time $T = t$." However, this is an epistemological, rather than ontological, uncertainty. In the same work, also a scalar difference between observables at different time points is computed, to indicate recurrences. Also, the Riemann sum is used, in a classical, non-quantum, framework, with applications in climatology and finance. Such probability recurrence definition has broad potential, e.g., when analysing paleoclimatetime series where dating uncertainties translate into proxy probabilities [10].

We also adopt a *kernel* technique. Kernel approaches have been used in forecasting [7]. Also, a strategy for retaining information on attractor geometry in nonlinear dynamics has been compared to a kernel density estimate [12]. Kernel methods have also been used in multi-dimensionality reduction problems via principal component analysis (PCA) [46]. Several approaches in the literature follow the structure: time series → distance → kernel similarity → recurrence analysis. However, the method that we will propose in this work, is: time series → distance → kernel similarity matrix → density matrix → principal eigenstate → quantum recurrence plot. The sequence distance → kernel → density matrix involves PCA and kernel similarity embedding, related to the approach in [46], and this constitutes a bridge with the literature on nonlinear analysis. In [17] it is used the kernel within the diffusion maps algorithm, together with the Koopman operators linearising the brain dynamics from fMRI in the space of functions, investigating low-dimensional manifolds where signals evolve. We highlight that, in existing kernel-based recurrence methods, the kernels modify the recurrence matrix. However, in our approach, the kernel is only an intermediate step to compute the density matrix that is used to build a new recurrence structure via the principal eigenstate. In fact, in our study, we use the principal eigenvector of the density matrix to represent the dominant mode of similarity within the encoded signal; from its amplitudes, we define scalar series, whose pairwise distances generate the recurrence structure.

While recurrence analysis has been applied to brain states, quantum recurrence analysis has yet to be explored in neuroscience. In this article, we propose its direct adaptation to natural time series from brain activity, measuring the equivalent of parameters such as purity and entropy, and thus sketching a first draft of quantum recurrence analysis (QRA) for neuroscience. In particular, here we provide a formal map from recurrence matrices to quantum density matrices, defined in the framework of open quantum systems [6], with two different reconstruction strategies; the introduction of quantum-inspired quantifiers and their application to brain time series from functional magnetic resonance, and finally the discussion of a possible link between the density-matrix distances and the K-operator, the *Krankheit–Operator* [31] describing some neurological disorders mostly as a connectomic alteration,

[1] While most of the literature uses directly the name *Alzheimer* to indicate the disorder, for historical reasons we prefer the double nomenclature, as also proposed by several scholars [26, 27, 41, 42], to recognise the contribution of Gaetano Perusini [44].

and thus relating operatorial algebra with insights on connectome-view of brain disease [50], and the wish for a unified theoretical approach encompassing computational results on different diseases [47].

As a general remark, we do not deal with quantum theories of the brain, which is a fascinating, yet controversial, research field, but we keep in mind that quantum-classical hybrids can be of great interest [48]. We would also clarify that here the term 'density matrix' is used in a purely mathematical sense, as a convenient representation induced by recurrence dynamics. This does not imply in any way the presence of quantum states in the neural tissue.

The idea of density matrix has already been adapted to non-quantum areas, with the definition of musical matrices as distribution matrices [29], and to characterise robotic swarms as a unique physical object [28]. Density matrices have also been used for recurrent neural network-based prediction [52] and to shape a quantum-like decision framework, of neuronal inspiration [23]. Finally, the K-operator was also used as an indicator to choose which area of the brain to focus attention on and where to continue the analysis with recurrence plots and joint recurrence plots [16].

The novelty of our work is the adaptation of a quantum-derived density-matrix idea to real, classical data of brain analysis, and the attempt to define a relationship with the K-operator.

3 Methods

We first present the definition of the recurrence matrix and of the density matrix, and then we present the method to encode time series into quantum states.

Definition 1 In the realm of classical physics, given a series of state vectors $\mathbf{x}(t)$, the Heaviside function Θ, and a threshold ε, the ijth element of the *recurrence matrix* $\mathbf{R}$ is defined as [34, 35, 43]:

$$R_{i,j} = \Theta(\varepsilon - \|\mathbf{x}_i - \mathbf{x}_j\|), \tag{1}$$

where $\|\cdot\|$ is a norm, and $\mathbf{x} \in \mathbb{R}^{n\times T}$ is the n-dimensional state vector ot length T. As an operator, we have the *recurrence operator* $R : \mathbb{R}^d \times \mathbb{R}^d \to \mathbb{R}$, whose matrix representation $\mathbf{R}$ has elements $R_{i,j}$ defined as in Eq. (1). The recurrence matrix is symmetric: $R_{ij} = R_{ji}$.

Some measurements can help characterise states, such as the recurrence rate RR, the density of recurrence points; the laminarity LAM, that is the percentage of recurrence points forming vertical lines in the recurrence plot, with minimal length $v_{\min} = 2$, and frequency distribution $P(v)$, and finally the determinism DET, the percentage of recurrence points forming diagonal lines in the recurrence plot, with minimal length $l_{\min} = 2$, and frequency distribution $P(l)$:

$$\mathrm{RR} = \frac{1}{N^2}\sum_{i,j=1}^{N} R(i,j), \quad \mathrm{LAM} = \frac{\sum_{v=2}^{N} vP(v)}{\sum_{v=1}^{N} vP(v)}, \quad \mathrm{DET} = \frac{\sum_{l=2}^{N} lP(l)}{\sum_{l=1}^{N} lP(l)}. \tag{2}$$

Definition 2 In the realm of quantum physics, where $|\psi\rangle$ characterises the state of a system, the *density operator* is defined as [6, 40]:

$$\rho = |\psi\rangle\langle\psi|, \tag{3}$$

whose ijth element is $\rho_{ij} = \langle i|\rho|j\rangle$, such that:

- ρ has unitary trace: $tr(\rho) = 1$;
- ρ is Hermitian;
- the eigenvalues of ρ are non-negative.

In the case of a mixture of states, Eq. (3) becomes [6]:

$$\rho = \sum_i p_i |\psi_i\rangle\langle\psi_i|, \tag{4}$$

where i indicates the state and p_i is a weight, with $0 \le p_i \le 1$ and $\sum_i p_i = 1$.

The evaluation of ρ helps distinguish between pure and mixed states: for mixed states, $tr(\rho^2) < 1$, else it is $= 1$. Pure states correspond to points on the surface of the Bloch sphere, while mixed states are inside it. Once the density matrices are computed, we can explore the meaning in our framework of the quantum *purity* [6], defined for a quantum state as:

$$\text{purity} \ = tr(\rho^2), \tag{5}$$

and of the von Neumann entropy using the eigenvalues of ρ:

$$S(\rho) = -tr(\rho \log(\rho)). \tag{6}$$

The purity provides information on how much a state is mixed: obviously, the higher the purity, the closer the state is to a pure state. In the framework of brain-data analysis, a low purity may characterise the presence of noise and (self-)desynchronisation within a time series.

In the following, we present a technique to encode time series into quantum states. It can be summarised as: time series $\rightarrow$ distance matrix $D \rightarrow$ kernel $k \rightarrow$ density matrix $\rho \rightarrow$recurrence. We start from the time series $\mathbf{x} = \{x_1, x_2, \ldots, x_T\} \in \mathbb{R}^T$ and normalise them. To map the distances between the elements of the initial time series into distances within a Hilbert-space representation [24], we introduce a positive-semidefinite kernel matrix $\mathbf{k}$ [46], defined as

$$k_{ij} = \exp\left(-\frac{D_{ij}^2}{2\sigma^2}\right), \tag{7}$$

where σ is a scale parameter. This is similar to the weighted RP approach in [15]. The kernel matrix is then normalised to obtain a valid density matrix:

$$\rho = \frac{k}{tr(k)}. \tag{8}$$

For quantum recurrence, we then consider the principal eigenvectors $|v_{\max}\rangle$ of ρ. It is an n-dimensional vector in the Hilbert space that encodes the relationships between all points of the density matrix. It is a geometric embedding of the overall time series, computed from the density matrix ρ. The statevector satisfies:

$$\rho v_{\max} = \lambda_{\max} v_{\max}, \tag{9}$$

which component-wise reads as:

$$\sum_{j=1}^{N} \rho_{ij} (v_{\max})_j = \lambda_{\max} (v_{\max})_i. \tag{10}$$

This is a *mixed* ρ. As a note, the ρ^* for only one dominant mode is:

$$\rho^* = \sum_i \lambda_i |v_i\rangle\langle v_i|. \tag{11}$$

Each component of $(v_{\max})_i$ corresponds to time point i. In quantum mechanics, if $|\psi\rangle = v_{\max}$, then the meaning of $|v_{\max},\, i|^2$ is the probability of being in the ith state. In our approach, $|v_{\max},\, i|^2$ corresponds to the "weight" of the information on time point i. Figure 1 shows ρ, $v_{\max,\, i}$, and ρ^* as heatmaps. In Appendix 1, visualisations of ρs and the principal eigenvectors for all the considered time series are provided. Then we encode $v_{\max}$ in a quantum state. How can we really interpret this statevector? The density matrix ρ encodes similarities between all points and the global structure of the time series. The principal eigenvector provides information on the dominant pattern of ρ. With $v_{\max}$, we can now compute the new distance matrix

$$\mathcal{D}_{ij} = |\,|(v_{\max})_i| - |(v_{\max})_j|\,|. \tag{12}$$

While the distance D_{ij} in Eq. (7) was a distance between time series points, measuring similarities within the original data space, the distance $\mathcal{D}$ defined in Eq. (12) is computed between the components of the eigenvector,

and provides a measure of the similarity in the Hilbert space. The described technique to obtain $\mathcal{D}$ is only a possible embedding of time series into a quantum framework, but not the only one. The steps to obtain quantum encoding of time series are illustrated in Algorithm 1. To perform the quantum encoding, a step of padding is often necessary, because quantum circuits require the statevector to have size 2^n, while our eigenvectors, derived from the time series, have length T that is different than a power of 2 in general. For this reason, the recurrence plots that we obtain from D_{ij} contain blocks of zeroes. The self-similarity of the corresponding elements is trivial. At this point, we can adapt the definition of density matrix for the quantum-encoded time series:

Definition 3 Let $\rho \in \mathbb{C}^{N\times N}$ be the density matrix obtained through the quantum encoding of a time series, and let $|v\rangle \in \mathbb{C}^N$ denote its principal eigenstate. Denoting with $\mathcal{D}_{\max} = \max_{k,l} \mathcal{D}_{kl}$ the maximum entry of $\mathcal{D}$, and with $\alpha \in [0, 1]$ a dimensionless threshold parameter, the ij-th element of the recurrence matrix for the quantum-encoded time series is

$$R_{ij} = \Theta(\alpha \mathcal{D}_{\max} - \mathcal{D}_{ij}) \tag{13}$$

where $\Theta(\cdot)$ denotes the Heaviside step function.

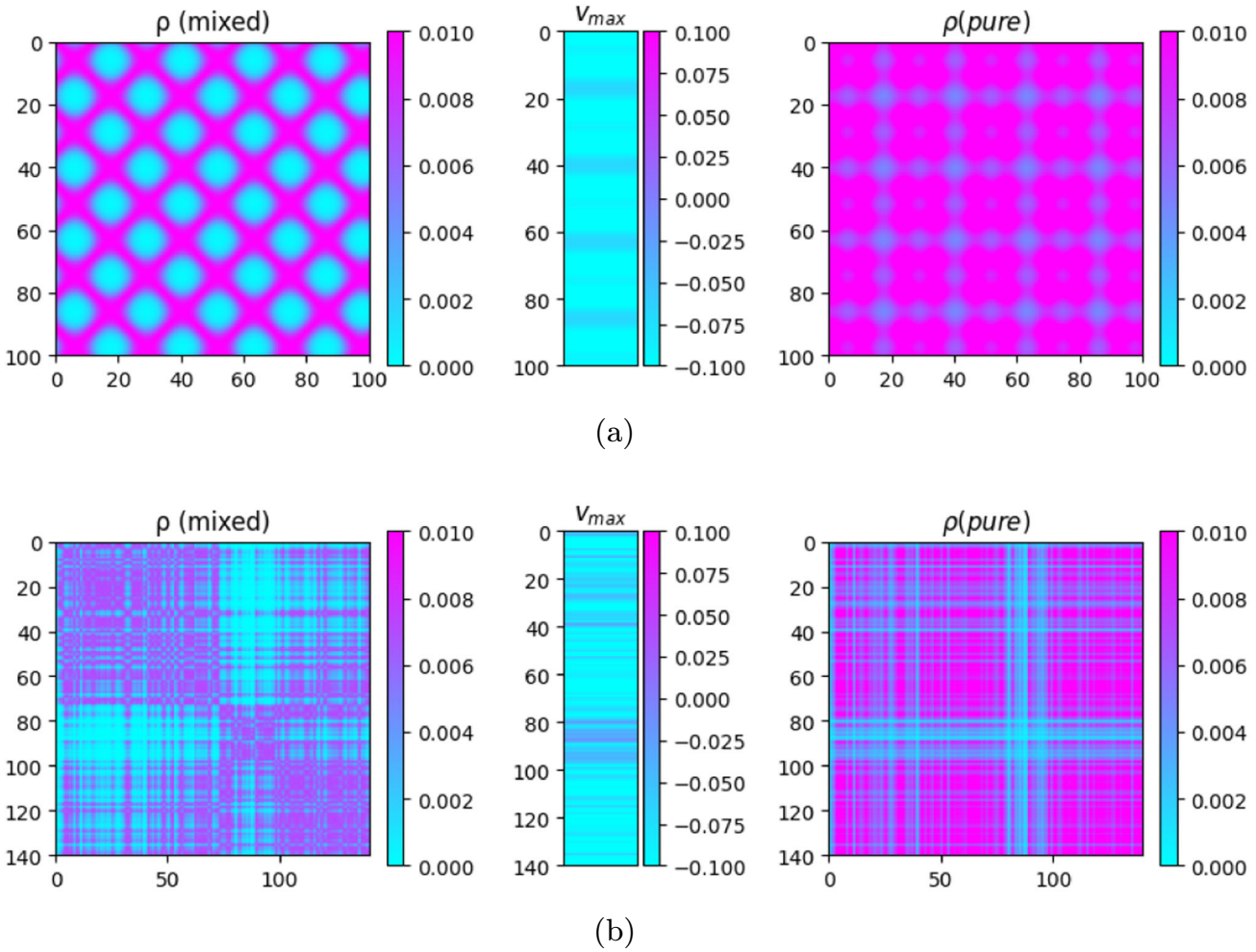


Fig. 1 ρ, the dominant component of $v_{\max}$, and ρ^* (real parts) for the time series of the sampled sinusoidal function $\sin(13/6)\pi x$ (**a**) and the insula of a healthy brain (**b**) are shown. We notice that, for (**a**), a second frequency already appears in v_{max}

Algorithm 1 Quantum-encoding strategy with density-matrix recurrence

Input: Time series $x = \{x_1, \ldots, x_T\}$, kernel $\kappa \in \{\text{rbf}, \text{rational}\}$, dimensionless threshold $\alpha \in [0, 1]$
Output: Density matrix ρ, recurrence matrix $\mathbf{R}$

(A) Distance construction
reshape x as column vectors
compute distance matrix $D_{ij}^{(x)} = \|\mathbf{x}_i - \mathbf{x}_j\|_2$

(B) Kernel construction
if σ not provided **then**
    let $\mathcal{S} = \{D_{ij}^{(x)} : i < j\}$
    $\sigma \leftarrow \max(\text{median}(\mathcal{S}), \varepsilon)$
end if
if $\kappa = \text{rbf}$ **then**
    $K_{ij} = \exp(-{D_{ij}^{(x)}}^2/(2\sigma^2))$
else if $\kappa = \text{rational}$ **then**
    $K_{ij} = 1/(1 + {D_{ij}^{(x)}}^2/\sigma^2)$
end if
symmetrise $K \leftarrow (K + K^\top)/2$

(C) Density matrix normalisation
$\rho \leftarrow K/\operatorname{tr}(K)$

(D) Quantum amplitude recurrence
compute principal eigenvector $v_{\max}$ of ρ
define quantum amplitude series $q_i = |(v_{\max})_i|$
compute distances $\mathcal{D}_{ij} = |q_i - q_j|$
$\mathcal{D}_{\max} \leftarrow \max_{k,l} \mathcal{D}_{kl}$
$R_{ij} \leftarrow \Theta(\alpha \mathcal{D}_{\max} - D_{ij})$

Finally, starting from our quantum-encoded states for each time series, we compute the von Neumann entropy of single-qubit reduced states, quantifying the distribution of correlations across the system. When the global state is pure, this coincides with the entropy of entanglement. We divide each state into two parts: one qubit, denoted by A, and the other qubits, denoted as a whole as B. The density matrix of the two parts are, respectively,

$$\rho_A = tr_B(\rho_{AB}), \quad \rho_B = tr_A(\rho_{AB}), \tag{14}$$

where tr_B denotes the *partial trace* operation with respect to system B, and tr_A the partial trace with respect to part A, and ρ_{AB} is the matrix for all qubits. If ρ_{AB} is a pure state, a measurement of the von Neumann entropy of the *reduced state*,

$$S(\rho_A) = -tr(\rho_A \log \rho_A), \tag{15}$$

greater than zero means that the state is entangled with the other qubits [6]. In our case, this can provide information on the (geometric) distinguishability between the time series. We can reiterate the process on all qubits, separating one qubit at a time from the others, and obtain a string of entropy values.

4 Results

As a simple example of how recurrence plots work, we can compare the recurrence plots (RPs) that can be obtained from a sinusoidal function and from a random one. In the first case, we notice a regular pattern of diagonals and nodes (Fig. 2(a)), while in the second case, the recurrence points are scattered (Fig. 11(g)). The determinism and laminarity values vary significantly between these examples, showing higher values for the sinusoidal function and lower values for the random one (Table 1).

For illustrative purposes, we also include the RPs obtained with the proposed quantum encoding technique, leading to representations reminiscent of the squares and blocks in the paintings of Piet Mondrian (1872–1944). A point on the quantum plot means that the ith and jth time points have similar contributions to the amplitudes

Table 1 Classical vs. quantum recurrence measures for the sinusoidal and the random functions of Fig. 2

Function	Domain	LAM	DET	RR	Purity	Entropy
$\sin\left(\frac{13}{6}\pi x\right)$	Classical ($\epsilon = 0.1$)	1.000	0.999	0.085	–	–
	Quantum ($\alpha = 0.1$) U	0.695	0.670	0.154	0.447	0.956
	Quantum ($\alpha = 0.1$) C	**0.392**	**0.372**	**0.081**	”	”
Random (seed 1)	Classical ($\epsilon = 0.1$)	0.116	0.133	0.069	–	–
	Quantum ($\alpha = 0.1$) U	0.537	0.520	0.159	0.433	1.110
	Quantum ($\alpha = 0.1$) C	**0.210**	**0.190**	**0.127**	”	”

U stands for uncorrected, and C stands for corrected

of the principal eigenvector of the density matrix. The regularity in the sinusoidal functions, by using Eq. (13), translates into thick black squares for a larger threshold, Fig. 2(c), or to a small black square and a regular pattern for a smaller threshold, Fig. 2(e). The quantum-encoded random RP presents vertical and horizontal lines and interruptions of the black pattern, Fig. 2(d), or a small black square and a random pattern for a large threshold, Fig. 2(f). Black off-diagonal regions may correspond to negligible quantum coherence between the time-indexed states, after the application of the kernel; however, their correct interpretation would require a dedicated study. The use of a kernel allows us to turn distances or recurrences into a positive-semidefinite similarity matrix, needed to define a valid quantum density matrix. The blocks that make the plots “Mondrian-like” do not indicate any intermittency of the signal, laminar phases, or modular organisation. Their presence is instead a consequence of the proposed computational approach, with the quantum-inspired recurrence, due to the combination of kernelisation, padding, with thresholding applied to density-matrix representations of the time series. In fact, the obtained density matrices present many of their rows and columns either identical or strongly correlated, because they encode global similarities of the signal. When computing the pairwise distances of the rows of the density matrix, we obtain large subsets of indices with very similar distance values. The positive-definite kernel further compresses these distances into a narrow range, and, finally, the thresholding operation maps these near-constant regions to uniform recurrence values. However, this does not constitute a problem, because this is a systematic effect for all time series. The blocks themselves should not be interpreted dynamically, but the areas outside them are still informative, as we will see for the real-world examples. *One can also wonder if the RQA measures have any meaning in themselves for quantum-encoded RPs.* There is also a risk that the recurrence measures might be dominated by these artefacts appeared with padding. To get rid of them, we used a correction, by truncating the quantum-encoded eigenvector to match the length of the original brain time series. Before moving to the real data, we present a comparison between LAM, DET, and RR for a sampled sinusoidal function and for a random time series, as well as values of purity and entropy for the quantum-encoded information, corresponding to the information provided in Fig. 2, see Table 1.

We notice that LAM, DET, and RR are higher for the sinusoidal function, but the difference is higher for the corrected quantifiers. In particular, the corrected value of DET for the quantum plot at $\alpha = 0.1$ is equal to 0.372, while for the random time series at $\alpha = 0.1$ as well is equal to 0.190. The use of quantum encoding replicates the difference in RR and allows us to estimate an equivalent of purity and entropy. In particular, entropy is higher for the random example, and the purity is smaller for the random than for the sinusoidal function, but the difference is small. For Table 1, we note that the deviations for the measurements based on quantum data are quite small. This likely reflects the presence of large black blocks. Future research may address the computation of the measurements by excluding them.

We now move towards the real data from the brain time series. The RPs for our selected cases are presented in Fig. 3. We observe the patterns of brain activity in the insula of three different individuals: a healthy person, number #018_S_4399 (female, 78 years old), Fig. 3(a), a patient (#A00015518, male, 60 y.o.) affected by schizophrenia, Fig. 3(b), and finally a patient (#019_S_5019, female, 63 y.o.) affected by AD, at the baseline, first, and second follow-up, respectively; see Fig. 3(c)–(e). The size of the selected sample is considerably restricted, and this limits the generalisability of our findings. The results obtained with the quantum encoding as the preprocessing step are obtained with the Qiskit qiskit.quantum_info,[2] and they are presented in Fig. 4. The comparison between classical and quantum-encoded recurrence analysis is presented in Table 2. A visualisation with barplots will be proposed in Fig. 10.

We notice that quantum LAM is higher for the healthy patient; the AD progression from the baseline to the second follow-up shows a progressive decrease in LAM, both for the classical and for the quantum encoding. Overall, the values of LAM and DET are higher for the quantum-encoded matrices without the correction. With the correction, that removes the artefacts induced by the padding, the trend is more clear. In particular, concerning

[2] https://quantum.cloud.ibm.com/docs/en/api/qiskit/quantum_info.

Table 2 Classical and quantum recurrence measures for the insula time series of the selected patients

Patient	Domain	Threshold	Correction	LAM	DET	RR	Purity	Entropy
Healthy	Classical	$\epsilon = 0.1$	–	0.615	0.509	0.207	–	–
	Quantum	$\alpha = 0.1$	✓	**0.365**	**0.280**	**0.111**	0.435	1.091
		0.1		0.894	0.873	0.262	”	”
		0.5	✓	**0.767**	**0.681**	**0.355**	”	”
		0.5		0.942	0.902	0.377	”	”
AD BL	Classical	$\epsilon = 0.1$	–	0.659	0.496	0.189	–	–
	Quantum	$\alpha = 0.1$	✓	**0.491**	**0.340**	**0.135**	0.432	1.111
		0.1		0.914	0.881	0.265	”	”
		0.5	✓	**0.858**	**0.784**	**0.394**	”	”
		0.5		0.945	0.907	0.391	”	”
AD FU1	Classical	$\epsilon = 0.1$	–	0.455	0.352	0.164	–	–
	Quantum	$\alpha = 0.1$	✓	**0.314**	**0.212**	**0.104**	0.434	1.080
		0.1		0.888	0.877	0.257	”	”
		0.5	✓	**0.713**	**0.639**	**0.349**	”	”
		0.5		0.942	0.915	0.378	”	”
AD FU2	Classical	$\epsilon = 0.1$	–	0.381	0.335	0.206	–	–
	Quantum	$\alpha = 0.1$	✓	**0.279**	**0.196**	**0.125**	0.436	1.122
		0.1		0.895	0.868	0.377	”	”
		0.5	✓	**0.630**	**0.573**	**0.365**	”	”
		0.5		0.866	0.843	0.265	”	”
Schizophrenic	Classical	$\epsilon = 0.1$	–	0.410	0.346	0.183	–	–
	Quantum	$\alpha = 0.1$	✓	**0.378**	**0.218**	**0.113**	0.435	1.112
		0.1		0.855	0.807	0.241	”	”
		0.5	✓	**0.745**	**0.650**	**0.390**	”	”
		0.5		0.918	0.876	0.377	”	”

Corrected quantum values remove the padding effect. Purity and entropy are computed from ρ

the AD patient, the progression from the baseline to the second follow-up shows a decrease of LAM (for $\alpha = 0.1$, $0.491 \rightarrow 0.314 \rightarrow 0.279$, and similarly for $\alpha = 0.5$, $0.858 \rightarrow 0.713 \rightarrow 0.630$), as well as DET (for $\alpha = 0.1$, $0.340 \rightarrow 0.212 \rightarrow 0.196$, and for $\alpha = 0.5$, $0.784 \rightarrow 0.639 \rightarrow 0.573$). Table 2 also includes values of quantum purity and entropy. The results obtained in this case differ from our expectations. However, this could be attributed to differences in quantum versus classical encoding of correlations. A purity of the healthy state (also in Table 2) can be lower than expected because the off-diagonal entries introduce mixing in the Hilbert space, and similarly, the entropy is subject to quantum correlations of our mathematical model. Values of purity and entropy do not change with α, as they are computed before the construction of the recurrence matrix.

As a methodological note, we prepared the quantum state corresponding to the dominant eigenvector of the density matrix ρ. No additional evolution or measurement are performed while building the new recurrence matrix and the recurrence plots. The quantum state provides a representation of the processed time series. With Qiskit's Statevector, we extract the statevector. Then, we proceed with a classical analysis. At the end of the Results section, we will also provide the measurements of the expectation values of two Pauli observables and the single-qubit reduced entropy.

4.1 Spectral analysis

We also compare the spectral configurations for the examples of Table 1. As a caveat, we highlight that the spectrum of the quantum-encoded signal is not a physical frequency spectrum. Instead, it comes from the adopted method to build the density matrix, and the meaning it carries is about the geometric similarity structure of the time series.

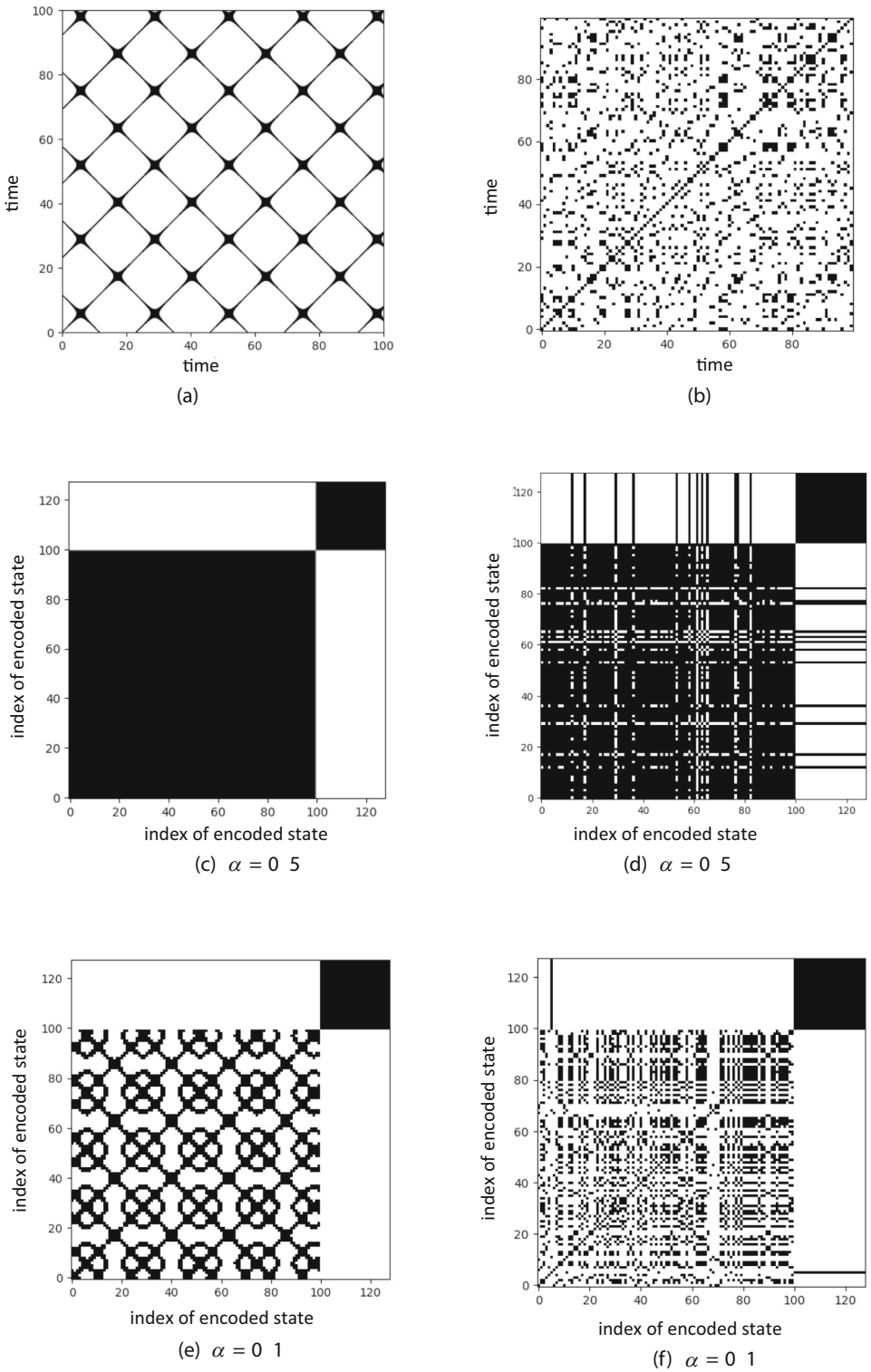
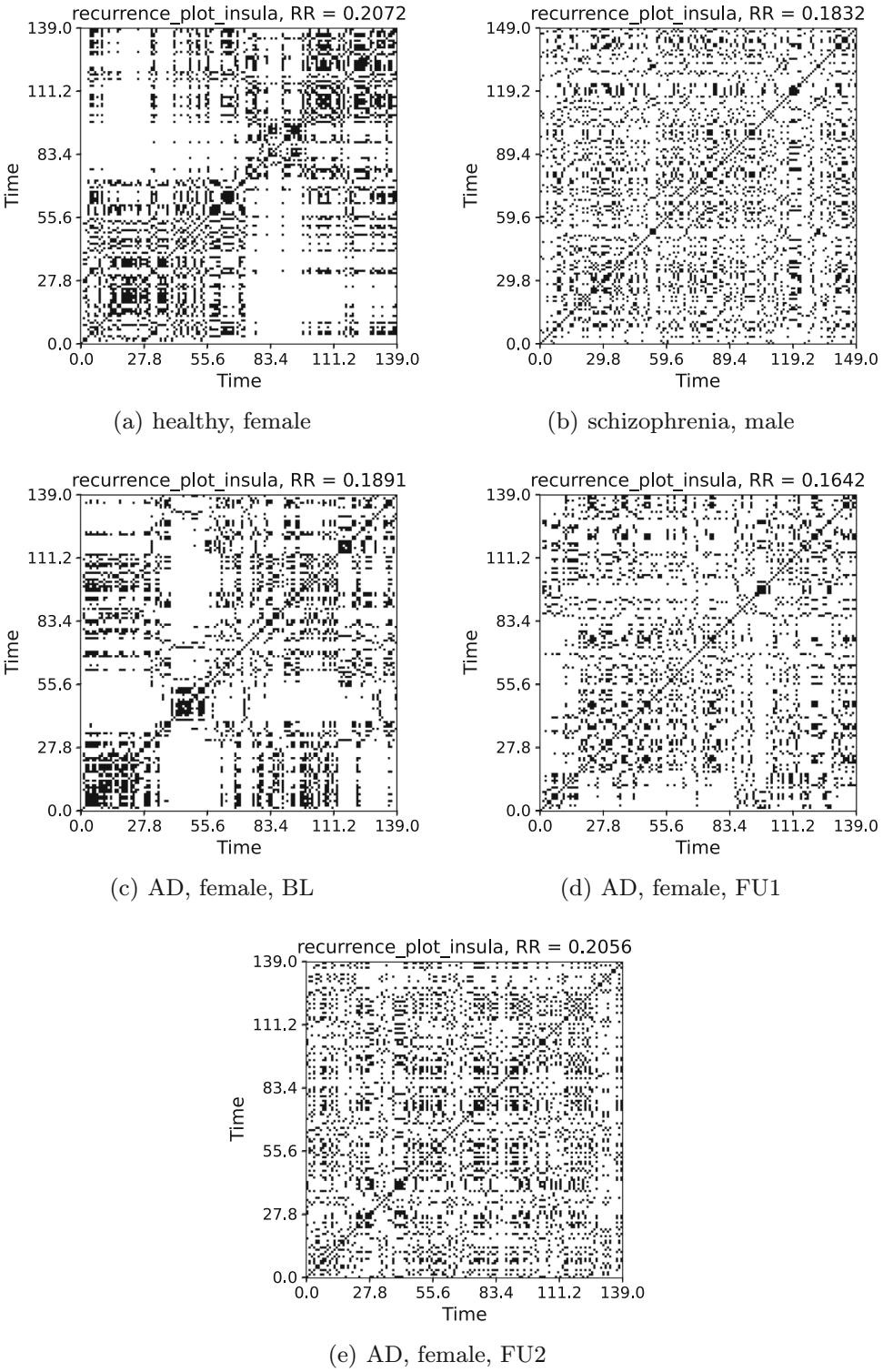


Fig. 2 Recurrence plots for two different cases: (**a**) function $\sin\left(\frac{13}{6}\pi x\right)$, and (b) random values, and their respective quantum encoding: from the sinusoidal function (**c**, **e**) and from the random one (**d**, **f**). For the quantum case, the axes represent indices of the density-matrix components. The black boxes in (**c**)–(**f**) correspond to the padding

We find that, concerning the sinusoidal signal, the one frequency is substituted by three main frequencies in the quantum domain; one of them shares a close x-value with the classical peak. The first quantum peak is higher, the other ones are lower (Fig. 5). For the random function, the distribution is different, but still there are multiple peaks as for the classical information, and overall, after the first, the quantum peaks are attenuated. Confirming the intuition from Fig. 2(e), the use of quantum encoding introduces more (mathematical) frequencies, as new spectral components added via the nonlinear transformation (kernel) and spectral projection (distances from the principal eigenvector).



(a) healthy, female

(b) schizophrenia, male

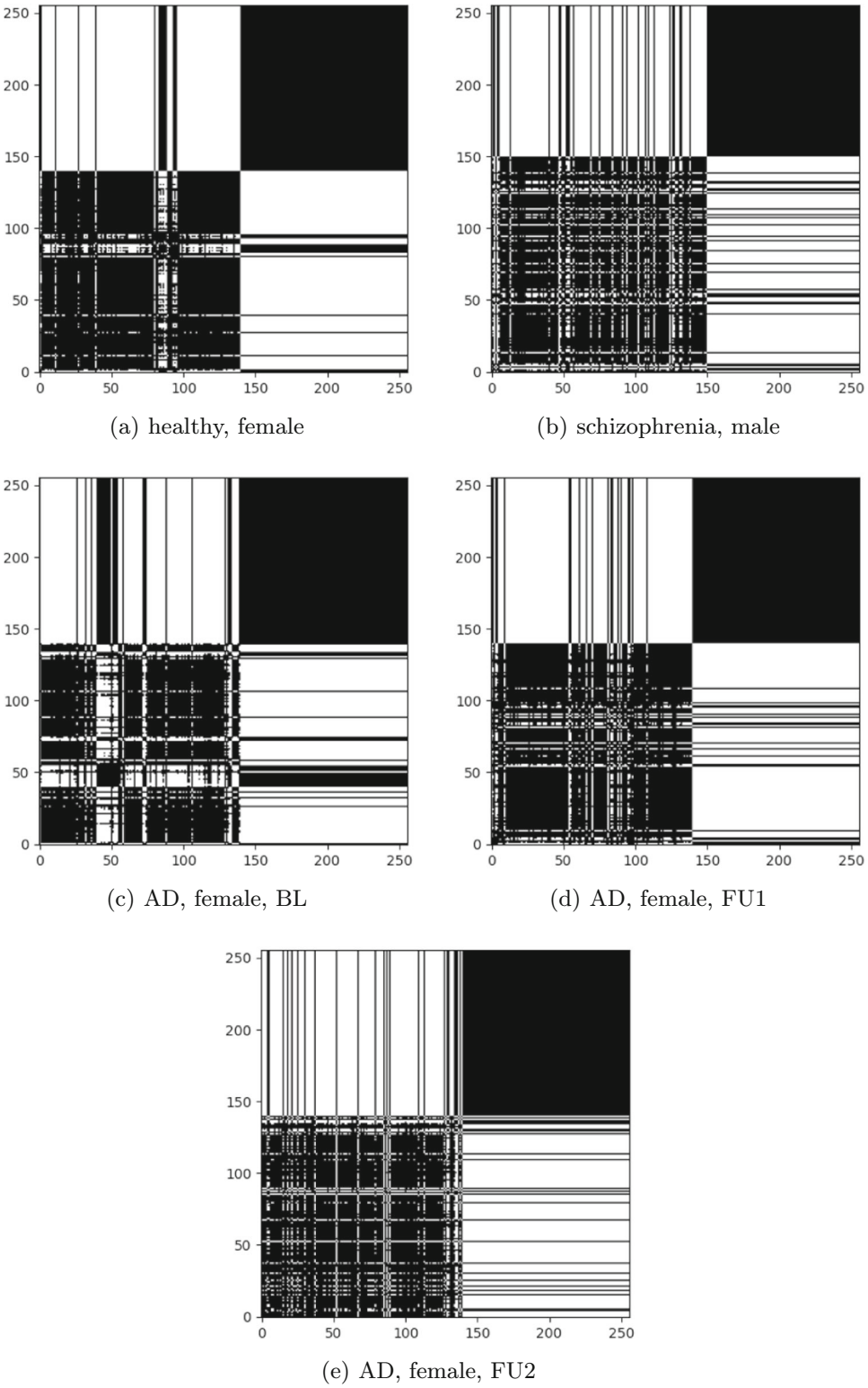
(c) AD, female, BL

(d) AD, female, FU1

(e) AD, female, FU2

Fig. 3 Recurrence plots (RPs) of the insula region for three representative cases: (**a**) healthy (female) subject, (**b**) schizophrenic (male) subject, Alzheimer–Perusini's disease (female) subject observed at the baseline (**c**), first (**d**), and second follow-up (**e**). All plots are computed using a threshold of 0.3

Then, we perform the same analysis for the real data (Fig. 6(c–g)). We notice that the quantum spectral pattern of the healthy brain area is more regular and, except the first, does not present any prominent peak. The quantum spectrum presents more homogeneity, for the healthy case, than the spectrum from the real-time series (Fig. 6(c)). The progression from the baseline to the first follow-up for the AD patient shows a clear increase of amplitudes of spectral component in the real-data signal. There is also a moderate increase of amplitude of the high-frequency components for the quantum-reconstructed signal, and a change of pattern following the progression of the disease (Fig. 6(d–f)). The differences are however less evident than for the real-time series. The more irregular pattern,



(a) healthy, female

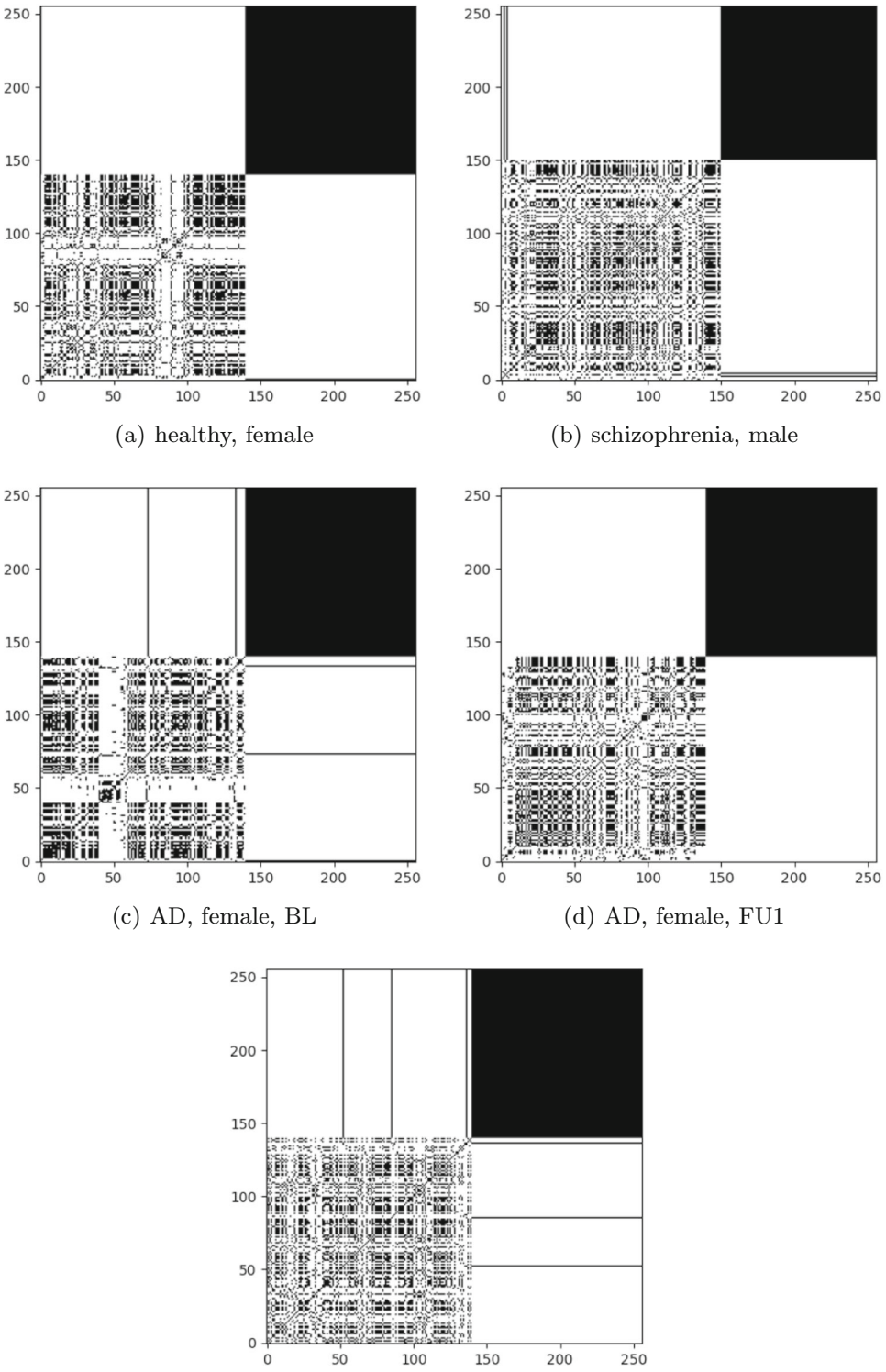
(b) schizophrenia, male

(c) AD, female, BL

(d) AD, female, FU1

(e) AD, female, FU2

Fig. 4 Recurrence plots from the quantum-encoded time series (QRPs) of the insula region for three representative cases: (**a**) healthy (female) subject, (**b**) schizophrenic (male) subject, Alzheimer–Perusini's disease (female) subject observed at the baseline (**c**), first (**d**), and second follow-up (**e**). All plots are computed using a value of α of 0.5. The axes contain the index of the encoded state. The black boxes correspond to the padding



(a) healthy, female

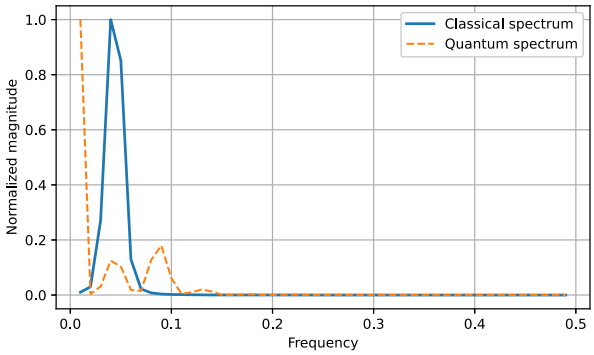
(b) schizophrenia, male

(c) AD, female, BL

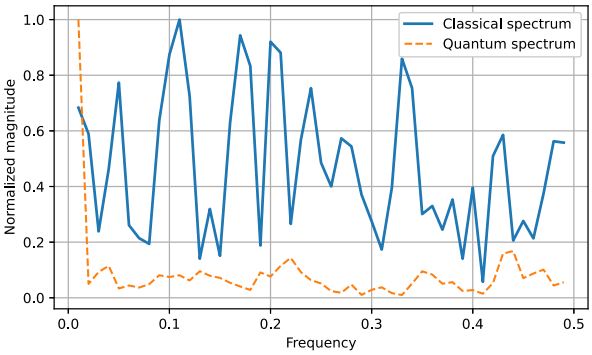
(d) AD, female, FU1

(e) AD, female, FU2

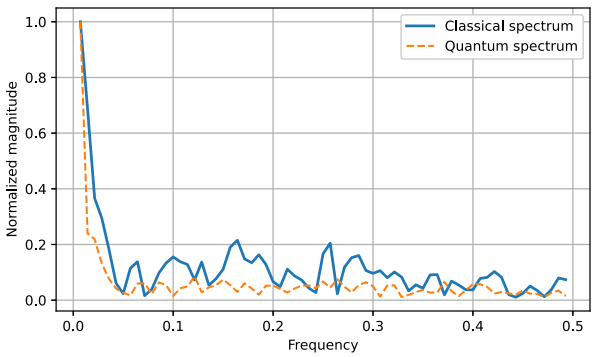
Fig. 5 Recurrence plots from the quantum-encoded time series (QRPs) of the insula region for the previous representative cases, computed with a value of α equal to 0.1. The black boxes correspond to the padding



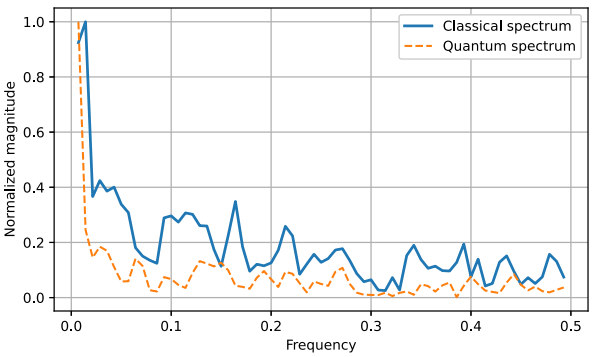
(a) sine



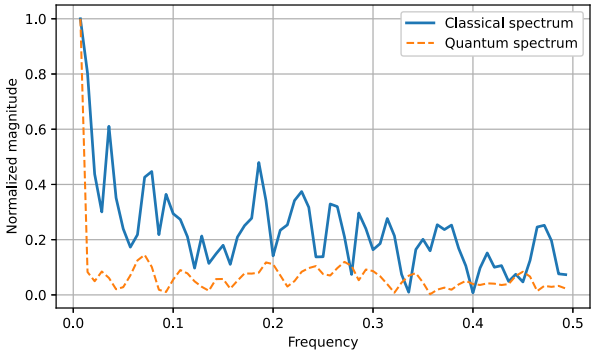
(b) random



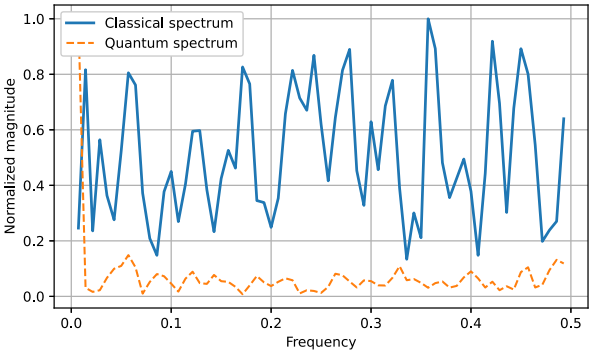
(c) healthy



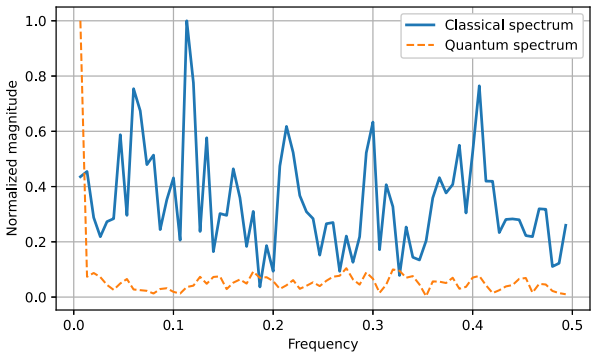
(d) AD, BL



(e) AD, FU1



(f) AD, FU2



(g) AD, schiz.

Fig. 6 Comparison of spectral distribution for the sample functions of Table 1, and for the real data of Table 2

with more abrupt oscillations of amplitudes of spectral components, is found for the signal of the schizophrenic brain, both for the classical and for the reconstructed quantum signal (Fig. 6(g)).

4.2 Parameter choice for the kernel

Until this point, we computed the kernel's σ from the lower triangular part of the square matrix D, and thus we used a slightly variable value for each matrix. In the following, we perform computations by first imposing the same value for all, and in particular by choosing a small one: $\sigma = 0.2$. The new recurrence plots are characterised by barcode-like patterns, which show an increase of density for the pathological cases, and especially for the progression of AD over time (Fig. 7). Also the presence of inner blocks is different, with a progressive disintegration of the small 4-block pattern for the healthy brain (Fig. 7(a)) to the 2nd follow-up of AD (Fig. 7(e)). In addition, we notice a stronger visual difference between the quantum recurrence plot of the schizophrenic brain (Fig. 7(b)) and the second follow-up for the AD brain (Fig. 7(e)), difference that was less evident also for the classical recurrence plots. The recurrence measures show a higher differentiation between the cases (Table 3). Interestingly, the value of quantum LAM for the schizophrenic brain area is 0.276, which is very close to the LAM of the quantum-code random signal, 0.285. Finally, the spectra also show a higher correspondence between the classical and the quantum case, with the instance of a central peak coincidence for the sine wave (Fig. 9(a)).

A comparative visualisation for the LAM, DET, RR values for the classical and corrected quantum plots is proposed in the barplots of Fig. 10.

4.3 Observable expectation values

We compute now the expectation values of the Pauli observables X and Z (satisfying $\langle Z\rangle^2 + \langle X\rangle^2 \leq 1$) from the statevector.

We first consider the expectation value of the Pauli operator acting on the first qubit (subscript 0). Let us start with the value obtained from the adaptive σ. We notice that, for the real data, the second follow-up of the AD presents the lowest value of $\langle X_0\rangle$, while its highest value is presented by the schizophrenic patient. We remark that these values characterise the geometry of the kernel-induced embedding, not the original signal directly. However, with the choice of $\sigma = 0.2$, pathological states present consistently the higher $\langle Z_0\rangle$ than the the healthy state, among the real data. In particular, the baseline of AD is the one with the highest $\langle Z_0\rangle$. A possible interpretation might hint towards an early sign of disease, highlighting a promising direction for future investigation. The second follow-up of AD shows the lowest value of $\langle X_0\rangle$. Synthetic signals appear as lying in a different range of values. With $\sigma = 0.2$, the separation between the states from the sinusoidal and random time series is more evident (Table 4).

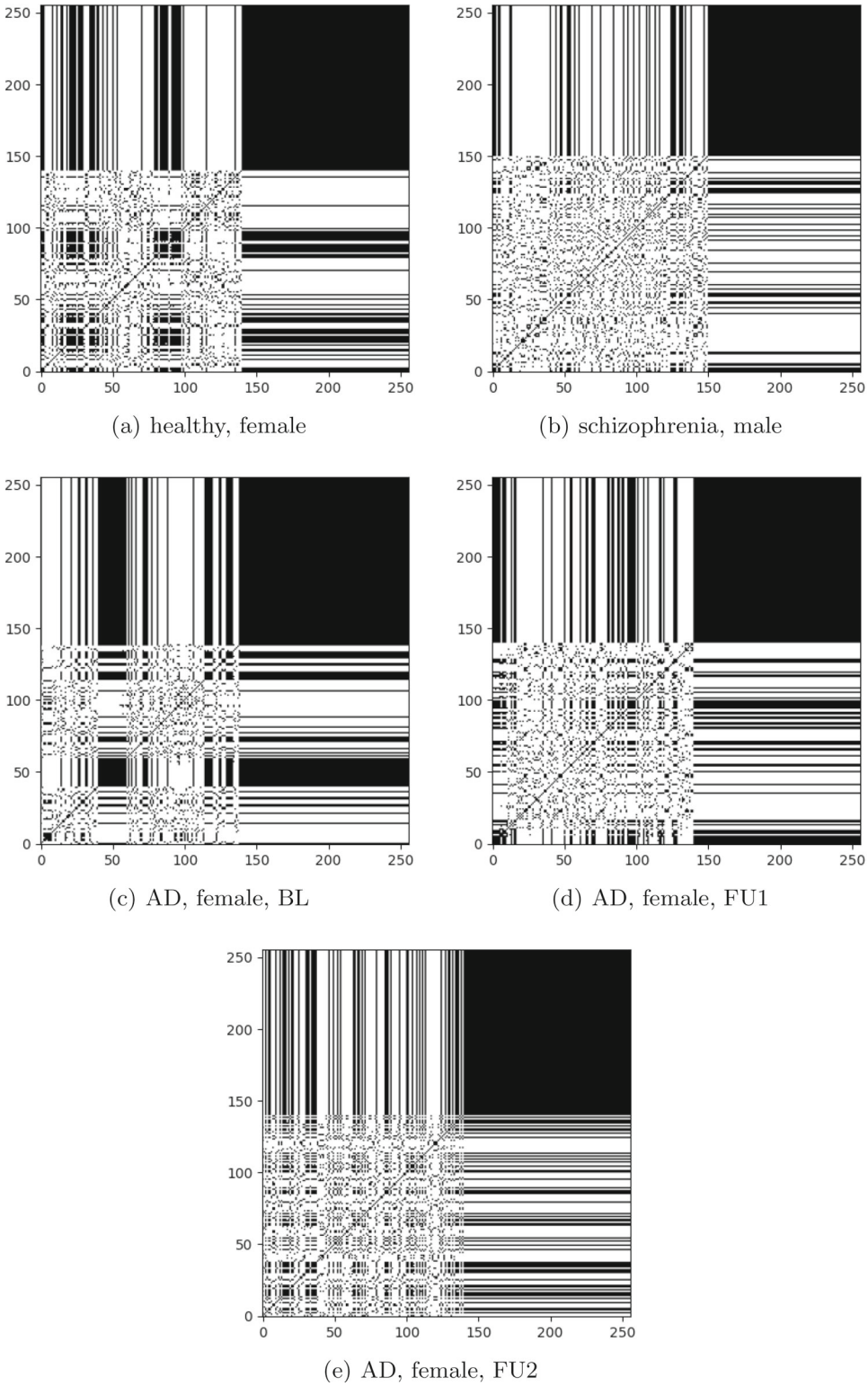
4.4 Entropy of single-qubit reduced states

We also show the values of entropies of single-qubit reduced states from the real-world data. We find that the entropies of the schizophrenic brain show a pattern of increasing values. A possible interpretation is a loss of modular structure. The progression of AD is reflected into a progressive flattening of the patterns of entropies, which can be interpreted as a loss of complexity. The healthy brain-derived qubits show a balance between the other trends. See Figure. 8 for their visualisation, and Table 5 for the corresponding values. The table also includes values for sine and random time series, whose single-qubit entropies show the most pronounced differences in the first two qubits, while, for higher qubits, the differences are smaller and less discriminative. Different values of σ lead to the same results.

These findings confirm that analysing the spread of information in disease-derived quantum encodings may effectively reveal patterns of brain activity. The results show that classifying brain disorders based on information spread, rather than mere activity levels, could constitute a viable approach.

5 Discussions

Further research can explore the implications of the quantum encoding technique and the definition of a suitable K-operator acting directly on time series, rather than on the elements of the connectivity matrices that can be derived from them. We can also explore eventual advantages of quantum encoding as a preprocessing step, also for the K-operator analysis, considering its action as the transformation of a healthy connectome, seen as a graph, into a diseased one, as another graph. More technical discussions on the idea of quantum graph state are provided in second Appendix.



(a) healthy, female

(b) schizophrenia, male

(c) AD, female, BL

(d) AD, female, FU1

(e) AD, female, FU2

Fig. 7 Recurrence plots from the quantum-encoded time series, computed with a value of α equal to 0.1, for a different choice of kernel ($\sigma = 0.2$). The black boxes correspond to the padding

Table 3 Classical and quantum recurrence measures for a different choice of σ in the kernel ($\sigma = 0.2$), and $\epsilon = 0.1$, $\alpha = 0.1$

Time series	Domain	LAM	DET	RR	Purity	Entropy
Healthy	Classical	0.615	0.509	0.207	–	–
	Quantum	0.443	0.306	0.112	0.124	2.355
AD BL	Classical	0.659	0.496	0.189	–	–
	Quantum	0.600	0.418	0.156	0.117	2.447
AD FU1	Classical	0.455	0.352	0.164	–	–
	Quantum	0.459	0.315	0.103	0.101	2.548
AD FU2	Classical	0.381	0.335	0.206	–	–
	Quantum	0.340	0.256	0.138	0.126	2.382
Schizophrenic	Classical	0.410	0.346	0.183	–	–
	Quantum	0.276	0.153	0.093	0.111	2.484
Sine	Classical	1.000	0.999	0.085	–	–
	Quantum	0.884	0.852	0.265	0.171	1.953
Random	Classical	0.116	0.133	0.069	–	–
	Quantum	0.285	0.197	0.104	0.118	2.405

Sinusoidal and random functions are defined as before. Quantum measurements are already corrected

Table 4 Expectation values of Pauli observables

Time series	Adaptive σ		$\sigma = 0.2$	
	$\langle Z_0 \rangle$	$\langle X_0 \rangle$	$\langle Z_0 \rangle$	$\langle X_0 \rangle$
Healthy	0.767	0.175	0.604	0.175
Schizophrenic	0.690	0.257	0.667	0.154
AD BL	0.856	0.147	0.948	0.068
AD FU1	0.777	0.147	0.698	0.060
AD FU2	0.885	0.116	0.868	0.049
Sine	0.283	0.714	0.232	0.389
Random	0.223	0.681	0.098	0.472

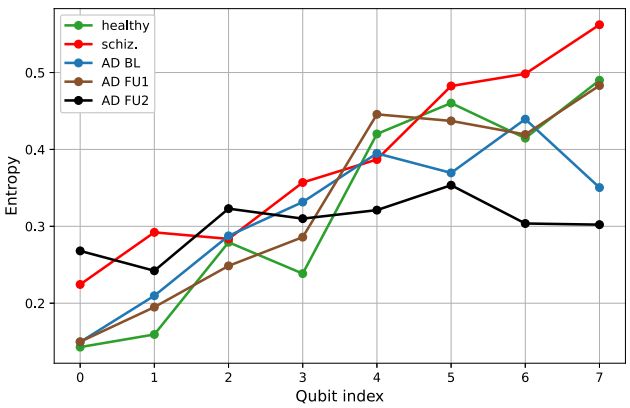


Fig. 8 Entropy of single-qubit reduced states

Table 5 Von Neumann entropy of single-qubit reduced states for the considered data

Qubit	Healthy	Schiz.	AD BL	AD FU1	AD FU2	Sine	Random
q_0	0.143	0.224	0.150	0.150	0.268	0.016	0.216
q_1	0.159	0.292	0.210	0.195	0.242	0.047	0.244
q_2	0.279	0.284	0.288	0.249	0.323	0.225	0.314
q_3	0.239	0.357	0.332	0.286	0.310	0.219	0.362
q_4	0.420	0.387	0.395	0.446	0.321	0.225	0.359
q_5	0.460	0.482	0.369	0.437	0.353	0.538	0.604
q_6	0.415	0.498	0.439	0.419	0.304	0.517	0.589
q_7	0.490	0.562	0.350	0.483	0.302	—	—

We can also think of the action of the K-operator on the activity of single brain areas, and not only on their connections, and thus indirectly transforming a recurrence matrix into another one. The action of K can be written in terms of different layers [31]:

$$K_{\text{weights of the connectome}} \otimes K_{\text{neuronal macro}-\text{agglomerate}} \otimes K_{\text{neuronal population}}. \tag{16}$$

Equation (16) follows the nested structure of the brain, composed of neurons, neuronal populations, neuronal macro-agglomerates, seen as nodes in the connectome. The elements $K_{\text{neuronal macro}-\text{agglomerate}}$, $K_{\text{neuronal population}}$ precisely lead to an alteration of the electric activity over time, disrupting the resulting time series. Consequently, K affects the recurrence matrices that can be derived from these time series. Because noise and temporal measurements have strong impact on the RP, one can almost never get an identical plot again, even when measuring a healthy person again. We can instead focus on the features of $\mathbf{R}$, such as line length distributions or the RQA measures. We can thus investigate the action of K on a matrix of features:

$$K^*_{\text{neuronal population}} \text{ Features } (\mathbf{R}_{\text{neuronal population}}) = \text{ Features } \left(\mathbf{R}^k_{\text{neuronal population}}\right), \tag{17}$$

where $\mathbf{R}$ is the recurrence matrix of a specific neuronal population of a healthy brain, $\mathbf{R}^k$ is the recurrence matrix of the same area affected by a neurological disorder, and $*$ denotes a suitable form of K. In previous studies, the K-operator was also adopted to find on which brain areas to further focus the attention, deepening the analysis with the recurrence plots [16]. Here, we are considering a direct action of a suitable form of K on the recurrence plots. As a further direction, we could envisage a quantum encoding at the level of the K-operator itself. Thus, jointly with a suitable version of the Grover's algorithm, K may help identify faster which brain areas are more impacted by the disease onset or by the disease progression.

Concerning the progression, if we consider the activity of a brain area encoded as a quantum state, the transition from a state to another one can be described as a path in the Hilbert space $\mathcal{H}$. Thus, a suitable version of K would drive such a path:

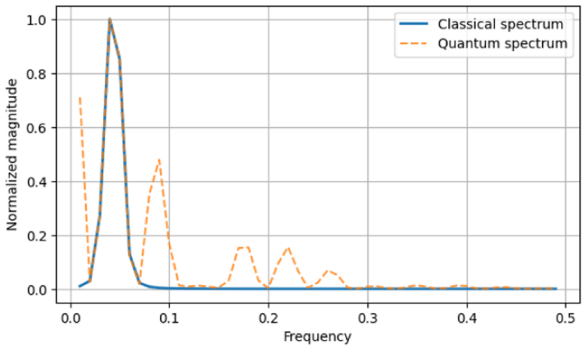
$$K^{\mathcal{H}}\rho_1 = \rho_2. \tag{18}$$

The path would be a quantum analogous of a path towards pathological points in the space of brain spaces [32].

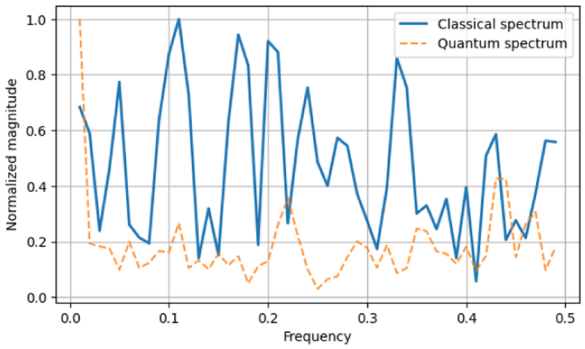
In this study, we proposed a more in-depth exploration of recurrences, including quantum-based ones. We completed the analysis with a comparison of the spectral distribution for the real brain signal and for the quantum-reconstructed one. The application of quantum computing can help speed up the proposed computations. The use of linear functions can speed up operations on $N \times N$ matrices, and quantum principal component analysis (qPCA) enables extracting dominant eigenmodes of low-rank density operators exponentially faster [21]. However, for the quantum application to be effective, some conditions have to be satisfied, for instance, efficient data-loading and control of noise that can disturb quantum states. We can safely consider the advantages that can be obtained with quantum-computational methods as an opportunity for future development, rather than an immediate option. Finally, having observed the spectral distribution from physical time series and quantum-encoded signals, we can sketch the following conjecture, pointing towards future research.

Conjecture 1 The method of kernel-based density-matrix encoding acts as a nonlinear spectral filter amplifying or reshaping recurrence structures.

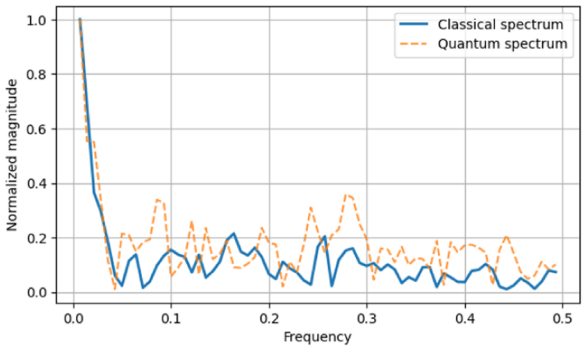
Research in these directions can allow us to develop new quantifiers potentially helpful in medical research, as well as to find new connections between mathematical objects of physics.



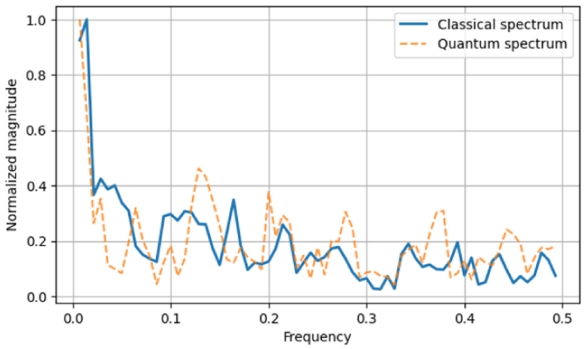
(a) sine



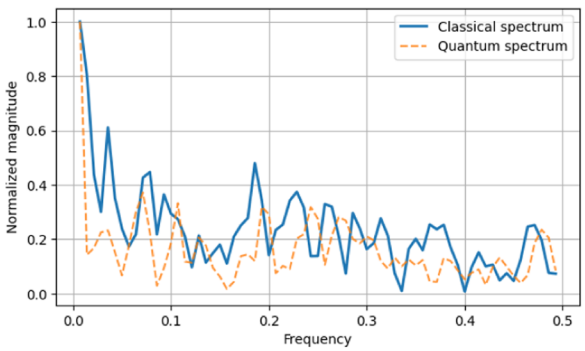
(b) random



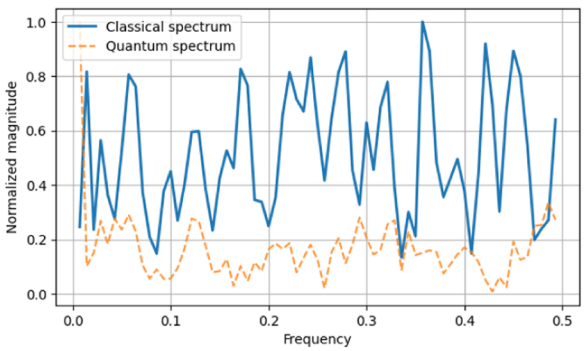
(c) healthy



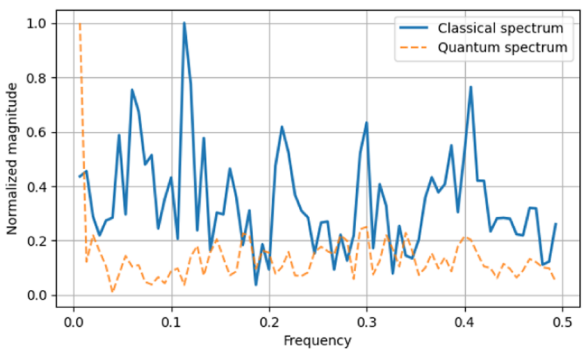
(d) AD, BL



(e) AD, FU1

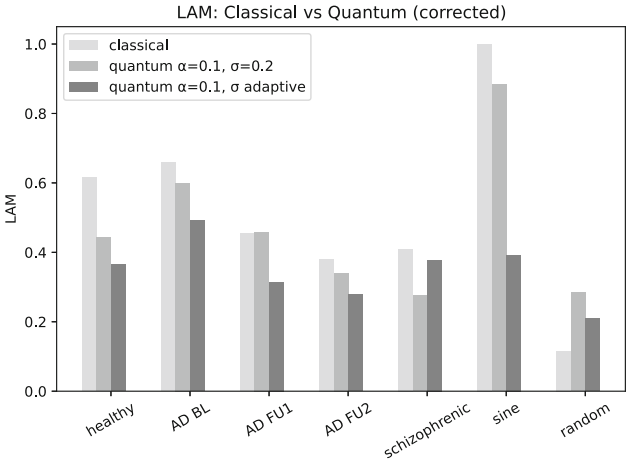


(f) AD, FU2

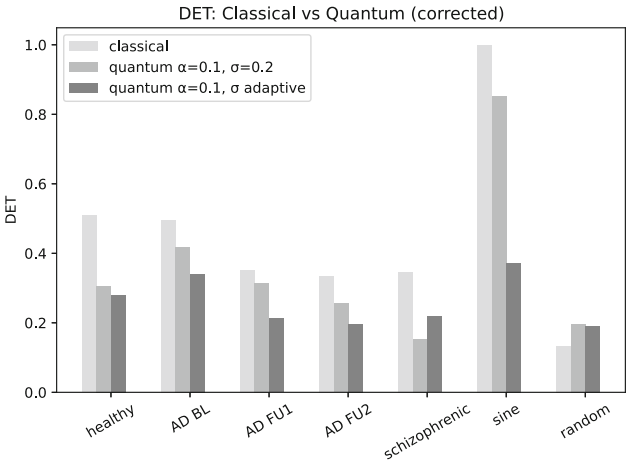


(g) AD, schiz.

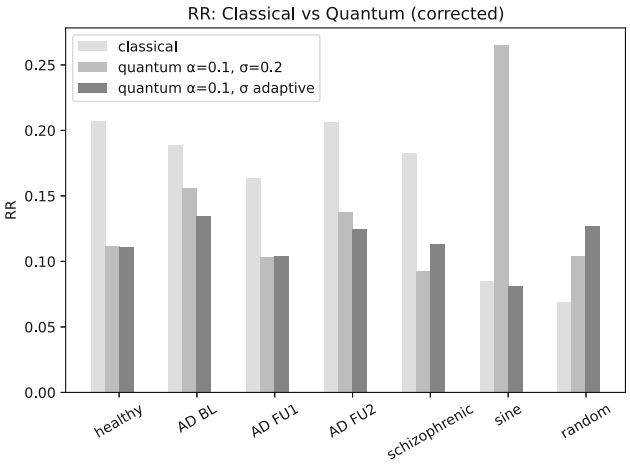
Fig. 9 Comparison of spectral distributions, $\sigma = 0.2$



(a)



(b)



(c) $\alpha = 0.2$

Fig. 10 Visual summary of the recurrence measurements, for classical and quantum (corrected) recurrence plots

6 Conclusions

In this article, we investigated patterns of behaviour of time series of a brain region through recurrence analysis. We focused on the insula for its importance concerning emotional processing and cognition. We also proposed and tested an approach based on quantum encoding of time series as a pre-processing step, comparing the measures obtained from the classical and the quantum-inspired analysis. By exploring the impact of choices of parameters for the kernel computation, we noticed that the quantum encoding can help differentiate the plot of the schizophrenic brain and the different stages, including the second follow-up, of the AD progression, where the classical recurrence plots were less characterised. To complete the analysis, we also assessed the expectation values of quantum observables, which, at least for the considered cases, might help discriminate between normal and pathological cases.

As an important *caveat*, entropy from quantum-encoded time series provides information on geometric similarity; it should not be interpreted as a biomarker of neural noise. And, as a limitation of the study, the empirical analysis was limited to selected patients of specific disorders. A larger sample of patients and healthy controls would be beneficial to strengthen and generalise the findings.

Funding Open access funding provided by Consiglio Nazionale Delle Ricerche (CNR) within the CRUI-CARE Agreement.

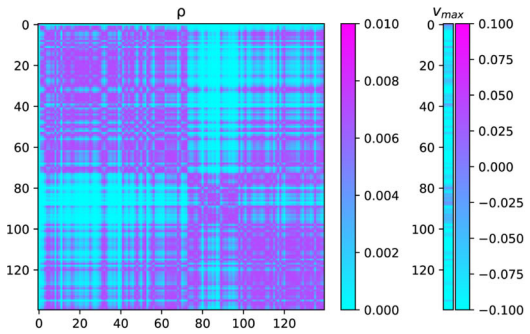
Data availability We considered an AD and a healthy control from the Alzheimer's Disease Neuroimaging Initiative (ADNI) database (https://adni.loni.usc.edu). As such, the investigators within the ADNI contributed to the design and implementation of ADNI and/or provided data but did not participate in the analysis or writing of this report. A complete listing of ADNI investigators can be found at: https://adni.loni.usc.edu/wp-content/uploads/how_to_apply/ADNI_Acknowledgement_List.pdf. Data from the patient affected by schizophrenia are derived from the COBRE dataset, http://schizconnect.org/.

Code availability The codes can be accessed at https://github.com/medusamedusa/recurrence_brain_states and https://codeberg.org/medusamedusa/quantum_recurrences/src/branch/main/. The codes to obtain NIfTI files from the original DICOM files are not included; they can be accessed from previous publications, such as [30]. The code to compute and visualise recurrence plots was adapted from https://pyts.readthedocs.io/en/latest/auto_examples/image/plot_single_rp.html, with original code by Johann Faouzi, licence: BSD-3-Clause. To compute laminarity and determinism, we used the package *pyunicorn* (Unified Complex Network and RecurreNce analysis toolbox) [11], https://www.pik-potsdam.de/~donges/pyunicorn/contact.html. Artificial intelligence has been used in the development of the methodological key points of quantum encoding (its content was then all verified and re-written by the authors) and for part of the codes.

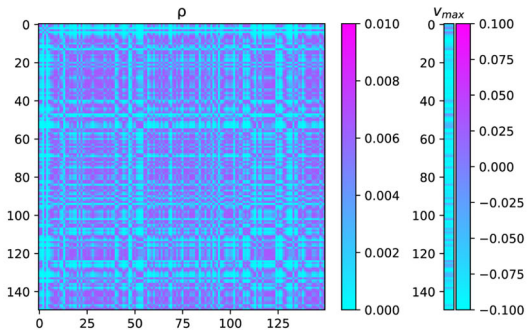
Open Access This article is licensed under a Creative Commons Attribution 4.0 International License, which permits use, sharing, adaptation, distribution and reproduction in any medium or format, as long as you give appropriate credit to the original author(s) and the source, provide a link to the Creative Commons licence, and indicate if changes were made. The images or other third party material in this article are included in the article's Creative Commons licence, unless indicated otherwise in a credit line to the material. If material is not included in the article's Creative Commons licence and your intended use is not permitted by statutory regulation or exceeds the permitted use, you will need to obtain permission directly from the copyright holder. To view a copy of this licence, visit http://creativecommons.org/licenses/by/4.0/.

Appendix 1: Density matrices and their principal eigenvectors

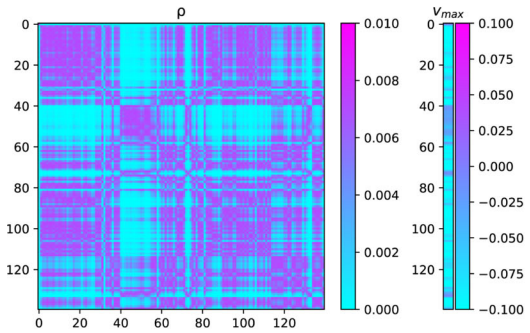
We provide here a visualisation of density matrices ρ and their principal eigenvectors as heatmaps, with the adaptive σ (Fig. 11) $\sigma = 0.2$ (Fig. 12). The latter shows plots more similar to the RPs: the density matrix is computed as a similarity matrix, and the value of σ is smaller, thus the action of the kernel is reduced.



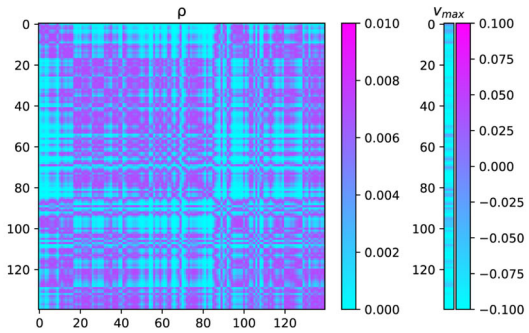
(a) Healthy



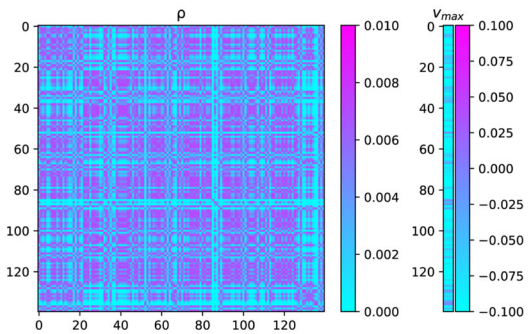
(b) Schizophrenia



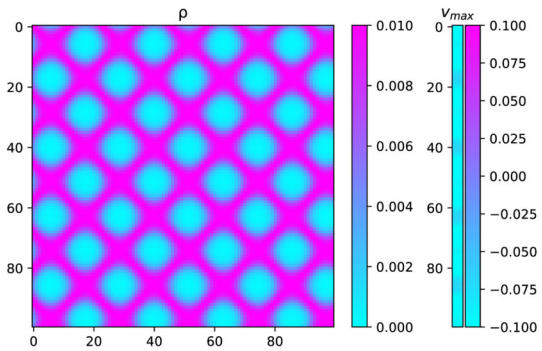
(c) AD baseline



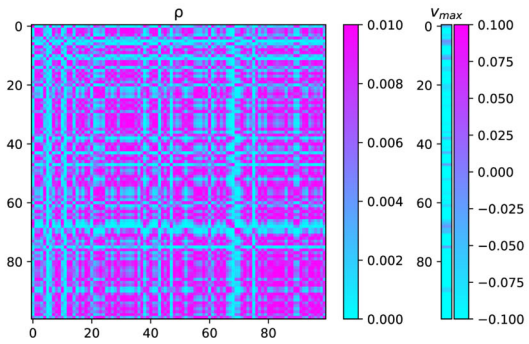
(d) AD follow-up 1



(e) AD follow-up 2

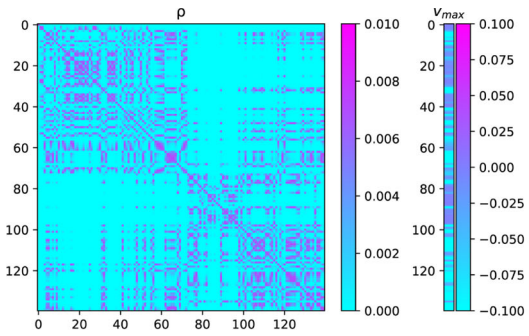


(f) Sine function

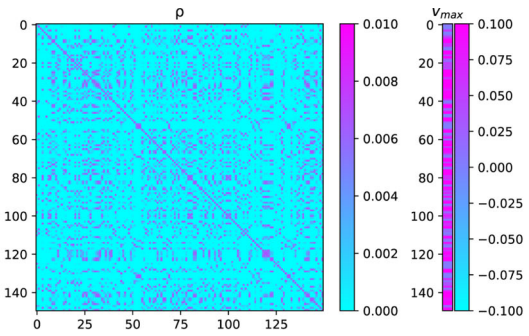


(g) Random

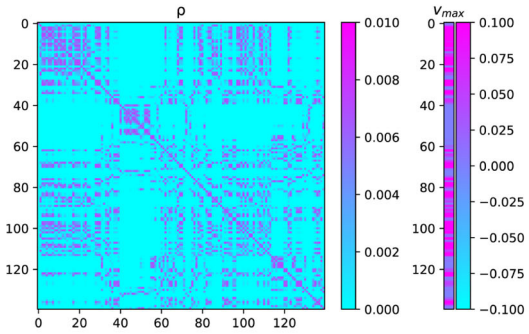
Fig. 11 ρ and $v_{max,\,i}$ (real part) for the considered time series. We consider the eigenvector with the largest eigenvalues



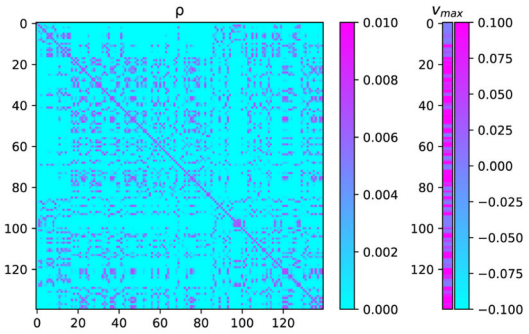
(a) Healthy



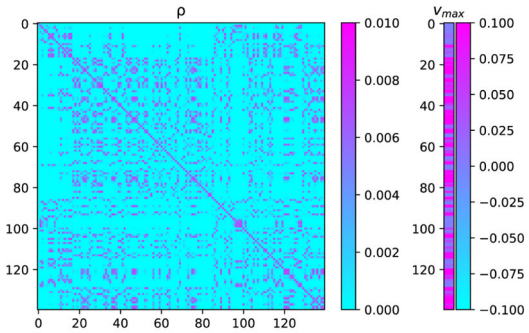
(b) Schizophrenia



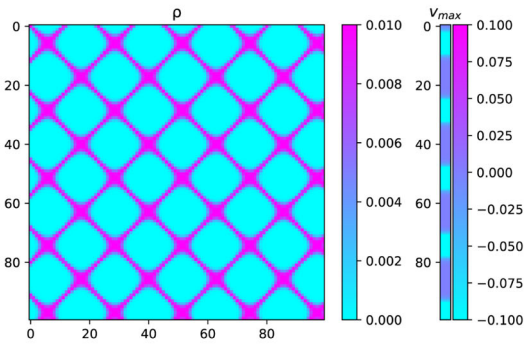
(c) AD baseline



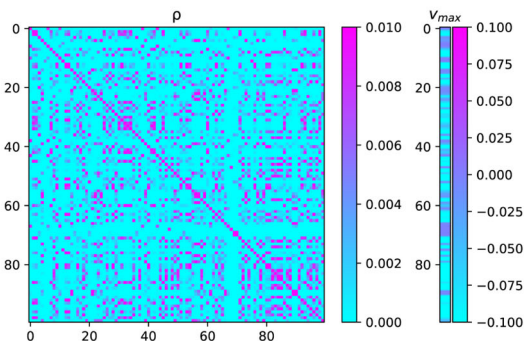
(d) AD follow-up 1



(e) AD follow-up 2



(f) Sine function



(g) Random

Fig. 12 ρ and $v_{\max}$ (real part) for the considered time series, with $\sigma = 0.2$

Appendix 2: Associativity matrix encoded as a quantum graph state

For the sake of completeness, we also include a reference to quantum graph states [18], independently of recurrence analysis. We extend the density-matrix perspective from time series in a brain region to network representation of the brain. Starting from the connectivity matrix of the overall brain, we focus on a pair of ROIs (namely, rectus and left insula), for reasons of computational limits. We encode the reduced matrix to a quantum multi-qubit state. Then, for this state, we compute ρ and thus the purity and entropy values for the insula by tracing on the other ROI. For the overall strategy, see Algorithm 2. Concerning the details, we can see the brain connectome as a graph $G(V, E)$, where the vertices of the graph represent the qubits, and the edges represent the action of controlled Z-gates. The graph is undirected if we consider the averaged signal exchaged between i- and jth nodes. According to [9, 37, 38, 53], referred in [18], we have:

$$|\psi_G\rangle = \Pi_{(i,j)\in E} CZ_{ij} |+\rangle^{\otimes V}, \tag{19}$$

with Z_{ij} is the controlled Z-gate acting on qubits $q[i]$ and $q[j]$. In [18], the author considers quantum graph states built via the action of 2-qubit gate $RXX(\psi_{ij}) = exp(-i\phi_{ij}\sigma_i^x\sigma_j^x/2)$, where $\sigma_i^x,\ \sigma_j^x$ are Pauli matrices that correspond to qubits $q[i],\ q[j]$ on a separable quantum state. Thus, the states are:

$$|\psi_G\rangle = \Pi_{(i,j)\in A} RXX_{ij}(\phi_{ij})|\psi_0\rangle. \tag{20}$$

These states can represent directed and weighted graphs, and they do not contain self loops. In our application, we have undirected but weighted graphs, and we can consider them as equally-directed graphs. From the obtained results, we notice that the normal brain shows intermediate values, while the AD baseline shows the highest purity and the lowest entropy, similar to the highest LAM concerning the classical measures (Table 6).

Table 6 Mapping each connectivity matrix to a quantum state graph in the sense of [18], then computing the density matrices, and the resulting values of purity and entropy

Patient	Purity	Entropy
AD BL	0.6891	0.4898
AD FU1	0.5257	0.6672
AD FU2	0.5722	0.6191
healthy	0.5595	0.6323
schizo	0.5363	0.6564

Algorithm 2 Two-node quantum graph state construction and analysis

Input: Connectivity matrix $C \in \mathbb{R}^{N\times N}$; Node indices i, j (here 27 and 28)
Output: Quantum circuit $\mathcal{C}$, full density matrix ρ, purity / entropy of full state and subsystems
Step 1: Extract the 2×2 correlation matrix
$C_2 \leftarrow C[\{i,j\},\{i,j\}]$
$r \leftarrow C_2(1,2)$
Step 2: Construct adjacency matrix A_2 from correlations
Map $[-1,1]$ to $[0,1]$
$A_2^{(1)} \leftarrow (C_2 + I)/2$; symmetrise
Step 3: Build Gnatenko graph-state circuit
Initialise 2-qubit circuit $\mathcal{C}$
for each qubit **do**
  Apply Hadamard gates H_0, H_1
  Compute RZZ rotation angle $\theta = 2A_2(1,2)$
  Apply $RZZ(\theta)$ between qubits $(0,1)$
end for
Step 4: Construct density matrix of the graph state
  Statevector $|\psi\rangle \leftarrow$ apply circuit $\mathcal{C}$. $\rho \leftarrow |\psi\rangle\langle\psi|$.
Step 5: Compute global purity and entropy
  Purity: $P = \mathrm{Tr}(\rho^2)$.
  Diagonalise ρ: $\rho = V\Lambda V^\dagger$.
  Von Neumann entropy: $S = -\sum_{\lambda_k>0} \lambda_k \log \lambda_k$.
Step 6: Compute reduced density matrix
  $\rho_1 \leftarrow \mathrm{Tr}_0(\rho)$ (trace out qubit 0).
Step 7: Compute subsystem purities and entropies
  $P_1 = \mathrm{Tr}(\rho_1^2), \quad S_1 = -\mathrm{Tr}(\rho_1 \log \rho_1)$

Considering the AD case, we can approximate the dynamics as the action of the K-operator on the states. This is the equivalent of defining the (pathological) dynamics between quantum graph state:

$$\mathcal{K}|_{a\,region}\colon \rho_{region}(t_0) \mapsto \rho_{region}(t_1) \mapsto \rho_{region}(t_2). \tag{21}$$

Finally, we can approximate the Liouville operator for the disease progression of the considered AD patient, see Eq. (22):

$$\mathcal{L}_{est} = \begin{pmatrix} 0.0+0.0i & 0.0+0.0i & \dots & 0.0+0.0i \\ -0.0015+0.0168i & 0.0094+0.0139i & \dots & -0.0015+0.0168i \\ \dots & \dots & \dots & \dots \\ 0.0+0.0i & 0.0+0.0i & \dots & 0.0+0.0i \end{pmatrix}; \tag{22}$$

this also approximates the action of the K-operator in its $\mathcal{K}^\circ$ variant, acting on density matrices. This operator is a linear Liouvillian, but not necessarily completely positive or in the Lindblad form.

References

1. A. Anand, D. Valluri, J. Davis, S. Ghose, Exact quantum recurrences in finite-dimensional floquet systems: an arithmetic and spectral framework (2025). https://arxiv.org/abs/2508.09933
2. M. Arioli et al., Action and emotion perception in Parkinson's disease: a neuroimaging meta-analysis. Neuroimage Clin. **35**, 103031 (2022)
3. M. Bergamino, E.G. Keeling, N.J. Ray, A. Macerollo, M. Silverdale, A.M. Stokes, Structural connectivity and brain network analyses in Parkinson's disease: a cross-sectional and longitudinal study. Front. Neurol. **14**, 1137780 (2023)
4. P. Bocchieri, A. Loinger, Quantum recurrence theorem. Phys. Rev. **107**, 337 (1957)
5. D.J. Bonthius, A. Solodkin, G.W. Van Hoesen, Pathology of the insular cortex in Alzheimer disease depends on cortical architecture. J. Neuropathol. Exp. Neurol. **64**(10), 910–922 (2005)
6. H.P. Breuer, E.M. Laine, J. Piilo, Measure for the degree of non-Markovian behavior of quantum processes in open systems. Phys. Rev. Lett. **103**(21040), 1 (2009)
7. D. Burov, D. Giannakis, K. Manohar, A. Stuart, Kernel analog forecasting: multiscale test problems. Multiscale Model. Simul. **19**(2), 1011–1040 (2021)

8. R.B. Buxton, The physics of functional magnetic resonance imaging (fMRI). Rep. Prog. Phys. **76**(9), 096601 (2013)
9. A. Cervera-Lierta, J.I. Latorre, D. Goyeneche, Exact multipartite entanglement of quantum states. Phys. Rev. A **100**, 022342 (2019)
10. J. Donath, Recurrence quantification analysis of probabilistic recurrence plots. Master's thesis, Humboldt University, Berlin (2019)
11. J.F. Donges, J. Heitzig, B. Beronov, M. Wiedermann, J. Runge, Q.-Y. Feng, L. Tupikina, V. Stolbova, R.V. Donner, N. Marwan, H.A. Dijkstra, J. Kurths, Unified functional network and nonlinear time series analysis for complex systems science: the pyunicorn package. Chaos **25**, 113101 (2015)
12. R.K. Donner, M. Small, J.F. Donges, N. Marwan, Y. Zou, R. Xiang, J. Kurths, Recurrence-based time series analysis by means of complex network methods. Int. J. Bifurc. Chaos **21**(4), 1019–1046 (2011)
13. J. Dudas, B. Carles, E. Plouet et al., Quantum reservoir computing implementation on coherently coupled quantum oscillators. npj Quantum Inf. **9**, 64 (2023)
14. J.-P. Eckmann, S. Oliffson Kamphorst, D. Ruelle, Recurrence plots of dynamical systems. Europhys. Lett. **4**(9), 973–977 (1987)
15. D. Eroglu, N. Marwan, S. Prasad, J. Kurths, Finding recurrence networks' threshold adaptively for a specific time series. Nonlinear Process. Geophys. **21**, 1085–1092 (2014)
16. S. Fazio, P. Ribino, F. Gasparini et al., k-operator for modelling neurodegeneration: simulations, fMRI application, eigenvalue analysis and recurrence plots. J. Med. Syst. **49**, 144 (2025). https://doi.org/10.1007/s10916-025-02244-6
17. I.K. Gallos, D. Lehmberg, F. Dietrich, C. Siettos, Data-driven modelling of brain activity using neural networks, diffusion maps, and the Koopman operator. Chaos **34**, 013151 (2024). https://doi.org/10.1063/5.0157881
18. K.P. Gnatenko, Entanglement of multi-qubit states representing directed networks and its detection with quantum computing. Phys. Lett. A **521**, 129815 (2024)
19. S. Goel, R. Agrawal, R.K. Bharti, Automated detection of epileptic EEG signals using recurrence plots-based feature extraction with transfer learning. Soft. Comput. **28**, 2367–2383 (2024)
20. B. Goswami, N. Boers, A. Rheinwalt, N. Marwan, J. Heitzig, S.F.M. Breitenbach, J. Kurths, Abrupt transitions in time series with uncertainties. Nat. Commun. **9**, 48 (2018). https://doi.org/10.1038/s41467-017-02456-6
21. A.W. Harrow, A. Hassidim, S. Lloyd, Quantum algorithm for linear systems of equations. Phys. Rev. Lett. **103**, 150502 (2009)
22. B. Karimi, X. Wu, A.N. Cleland, J.P. Pekola, A blueprint for experiments exploring the Poincaré quantum recurrence theorem. Phys. Rev. Res. **8**, L012062 (2026). https://doi.org/10.1103/wv9h-x14y
23. A. Khrennikov, I. Basieva, E.M. Pothos et al., Quantum probability in decision making from quantum information representation of neuronal states. Sci. Rep. **8**, 16225 (2018)
24. G. Kimura, The Bloch vector for N-level systems. Phys. Lett. A **314**(5–6), 339–349 (2003)
25. F.E.L. Lopes da Cruz, T. de Lima Prado, S.R. Lopes, N. Marwan, J. Kurths, Density-based recurrence measures from microstates. Phys. Rev. E **111**, 044212 (2025)
26. B. Lucci, The contribution of Gaetano Perusini to the definition of Alzheimer's disease. Ital. J. Neurol. Sci. **19**, 49–52 (1998). https://doi.org/10.1007/BF03028813
27. G. Macchi, C. Brahe, M. Pomponi, Alois Alzheimer and Gaetano Perusini: should man divide what fate united? Behav. Neurol. **10**(4), 105–108 (1997). https://doi.org/10.3233/BEN-1997-10401
28. M. Mannone, M. Anand, P. Fazio, A. Swikir, Density matrix-based dynamics for quantum robotic swarms. Robot. Auton. Syst. **200**, 105418 (2026). https://doi.org/10.1016/j.robot.2026.105418
29. M. Mannone, G. Compagno, Characterisation of the degree of musical non-Markovianity. J. Creat. Music Syst. (2022). https://doi.org/10.5920/jcms.975
30. M. Mannone, P. Fazio, J. Kurths, P. Ribino, N. Marwan, A brain network operator for modeling disease: a first data-based application for Parkinson's disease. Eur. Phys. J. Spec. Top. (2024). https://doi.org/10.1140/epjs/s11734-024-01345-6
31. M. Mannone, P. Fazio, N. Marwan, Modeling a neurological disorder as the result of an operator acting on the brain: a first sketch based on network channel modeling. Chaos **34**, 053133 (2024). https://doi.org/10.1063/5.0199988
32. M. Mannone, P. Ribino, P. Fazio, N. Marwan, Sketching a space of brain states. Neuroinformatics (2025). https://doi.org/10.1007/s12021-025-09739-0
33. N. Marwan, K.H. Kraemer, Trends in recurrence analysis of dynamical systems. Eur. Phys. J. Spec. Top. **232**, 5–27 (2023)
34. N. Marwan, J. Kurths, Nonlinear analysis of bivariate data with cross recurrence plots. Phys. Lett. A **302**(5–6), 299–307 (2002)
35. N. Marwan, M.C. Romano, M. Thiel, J. Kurths, Recurrence plots for the analysis of complex systems. Phys. Rep. **438**(5–6), 237–329 (2007)
36. N. Marwan, N. Wessel, U. Meyerfeldt, A. Schirdewan, J. Kurths, Recurrence-plot-based measures of complexity and their application to heart-rate-variability data. Phys. Rev. E **66**, 026702 (2002)
37. R. Mezher, J. Ghalbouni, J. Dgheim, D. Markham, Efficient quantum algorithms for entanglement measures. Phys. Rev. A **97**, 022333 (2018)
38. G.J. Mooney, C.D. Hill, L.C.L. Hollenberg, Entanglement-assisted quantum recurrence analysis. Sci. Rep. **9**, 13465 (2019)

39. E.J. Ngamga, S. Bialonski, N. Marwan, J. Kurths, C. Geier, K. Lehnertz, Evaluation of selected recurrence measures in discriminating pre-ictal and inter-ictal periods from epileptic EEG data. Phys. Lett. A **380**(16), 1419–1425 (2016)
40. M.A. Nielsen, I.L. Chuang, *Quantum Computation and Quantum Information* (Cambridge University Press, Cambridge, 2010)
41. F. Pellegrini, M. Mutali Jr., M. Zeppieri, The short and brave life of Gaetano Perusini: a tribute to his role in shaping neuroscience. Cureus **16**(2), e54240 (2024). https://doi.org/10.7759/cureus.54240
42. F. Pellegrini, M. Rosso, D.T. Chu, Gaetano Perusini: the forgotten neuroscientist "Alzheimer's" disease. Neuroscientist. **29**(3), 273–276 (2021). https://doi.org/10.1177/10738584211059466
43. A. Pentari, G. Tzagkarakis, P. Tsakalides, P. Simos, G. Bertsias, E. Kavroulakis, K. Marias, N.J. Simos, E. Papadaki, Changes in resting-state functional connectivity in neuropsychiatric lupus: a dynamic approach based on recurrence quantification analysis. Biomed. Signal Process. Control **84**, 104843 (2023)
44. G. Perusini, Über klinisch und histologisch eigenartige psychische Erkrankungen des späteren Lebensalters. Histologische und pathologische Arbeiten über die Grosshirnrinde mit besonderer Berücksichtigung der pathologischen Anatomie der Geisteskrankheiten **3**, 297–351 (1910). https://archive.org/details/b21909441_0003/page/298/mode/2up
45. G.M. Ramírez Ávila, A. Gapelyuk, N. Marwan, T. Walther, H. Stepan, J. Kurths, N. Wessel, Classification of cardiovascular time series based on different coupling structures using recurrence networks analysis. Phil. Trans. R. Soc. A **371**(1997), 20110623 (2013)
46. B. Schölkopf, A. Smola, K.-R. Müller, Nonlinear component analysis as a kernel eigenvalue problem. Neural Comput. **10**(5), 1299–1319 (1998)
47. W.W. Seeley, Mapping neurodegenerative disease onset and progression. Cold Spring Harb. Perspect. Biol. **9**, a023622 (2017)
48. A. Sergi, A. Messina, C.M. Vicario, G. Martino, A quantum–classical model of brain dynamics. Entropy **25**(4), 592 (2023). https://doi.org/10.3390/e25040592
49. J.M. Sheffield, B.M. Rogers, J. Urbano Blackford, S. Heckers, N.D. Woodward, Insula functional connectivity in schizophrenia. Schizophr. Res. **220**, 69–77 (2020)
50. C. Stam, Modern network science of neurological disorders. Nat. Rev. Neurosci. **15**, 683–695 (2014)
51. N. Tzourio-Mazoyer, B. Landeau, D. Papathanassiou, F. Crivello, O. Etard, N. Delcroix, E.T. Rolls, C. Huang, C. Lin, J. Feng, B. Mazoyer, M. Joliot, Automated Anatomical Labeling (AAL1) atlas [Dataset]. Human Brain Project Neuroinformatics Platform (2020)
52. J.D. Viqueira, D. Faílde, M.M. Juane, A. Gómez, D. Mera, Density matrix emulation of quantum recurrent neural networks for multivariate time series prediction. Mach. Learn. Sci. Technol. **6**(1), 015023 (2025)
53. Y. Wang, Y. Li, Z. Yin, B. Zeng, Quantum algorithm for simulating the dynamics of open quantum systems. Npj Quantum Inf. **4**, 46 (2018)
54. S. Zeemering, K. Borof, U. Schotten, J. Obergassel, A.J. Camm, H.J.G.M. Crijns, L. Eckardt, L. Fabritz, A. Goette, Z. Habibi, J. Heijman, B.J.M. Hermans, M.D. Lemoine, C. Magnussen, A. Metzner, A. Rillig, R.B. Schnabel, E. Schuijt, A. Suling, P. Vardas, S. Willems, A. Zapf, P. Kirchhof, Estimated atrial fibrillation burden on early rhythm-control and cardiovascular events in the EAST-AFNET 4 trial. Eclinicalmedicine **88**, 103457 (2025)
55. Y. Zhang, W. Zhou, J. Huang, B. Hong, X. Wang, Neural correlates of perceived emotions in human insula and amygdala for auditory emotion recognition. Neuroimage **260**, 119502 (2022)